

Journal of Materials Chemistry C

Accepted Manuscript



This is an *Accepted Manuscript*, which has been through the Royal Society of Chemistry peer review process and has been accepted for publication.

Accepted Manuscripts are published online shortly after acceptance, before technical editing, formatting and proof reading. Using this free service, authors can make their results available to the community, in citable form, before we publish the edited article. We will replace this *Accepted Manuscript* with the edited and formatted *Advance Article* as soon as it is available.

You can find more information about *Accepted Manuscripts* in the [Information for Authors](#).

Please note that technical editing may introduce minor changes to the text and/or graphics, which may alter content. The journal's standard [Terms & Conditions](#) and the [Ethical guidelines](#) still apply. In no event shall the Royal Society of Chemistry be held responsible for any errors or omissions in this *Accepted Manuscript* or any consequences arising from the use of any information it contains.

COMMUNICATION

Effects of Side Groups on Kinetics of Charge Carrier Recombination in Dye Molecule-Doped Multilayer Organic Light-Emitting Diodes

Cite this: DOI: 10.1039/x0xx00000x

Received 00th January 2012,
Accepted 00th January 2012

DOI: 10.1039/x0xx00000x

www.rsc.org/

Shengwei Shi,^{*,ab} Feng Gao,^b Zhengyi Sun,^b Yiqiang Zhan,^c Mats Fahlman,^b and Dongge Ma^a

The carrier recombination coefficient (γ) in dye molecule-doped multilayer organic light-emitting diodes was quantified by transient electroluminescence. It was found that γ and device efficiency were both strongly dependent on the molecular structures of the dopants.

Organic light-emitting diodes (OLEDs) have been extensively studied for their promising applications in flexible displays,¹ and solid state lighting.^{2,3} High performance organic materials, new device structures and advanced processing technologies are developed to advance the development of the OLED community.⁴⁻⁶ So far, OLEDs are the most successful application of organic semiconductors. It is well acknowledged that electrical processes in OLEDs include three key steps, i.e. charge injection, charge transport, and charge carrier recombination. All of these three processes play very important roles in device performance.⁷⁻¹¹

Transient electroluminescence (EL) (time resolved EL) has been widely used to investigate the electrical processes in OLEDs, enabling us to analyse charge transport and recombination in OLEDs.¹²⁻²² When a square voltage pulse is applied over the device, the EL starts to rise with a time delay, which has been interpreted as the transit time of the majority charge carriers. As the RC time constant of the setup is well below the delay time, it is unlikely that the RC constant is responsible for the delay time. The interpretation of the response time of the device in terms of transit time gives the mobility value.¹²⁻¹⁸ When the square voltage pulse is removed, the EL starts to decay, and it gradually decreases to zero EL. This decay time is closely related with bimolecular recombination of electrons and holes. The recombination coefficient (γ) then can be obtained from the decay part in transient EL,¹⁹⁻²¹ which is considered to be very important to understand the operating mechanism in OLEDs. However, most mechanistic investigations of OLEDs from transient EL are focused on the simple structure of electron-transport

layer/emissive layer/hole-transport layer;¹²⁻²¹ there are very less device physics studies on the multilayer structure,²² which is adopted in practical applications. In addition, although many highly efficient molecules are developed in OLEDs, with different side groups to adjust the solubility,²³ suppress the crystallization at ITO/organic interface,²⁴ reduce concentration quenching in phosphorescence,²⁵ or inhibit the aggregation light-emission,²⁶ it is still not clear how these side groups affect the device efficiency from the understanding of device physics.

In this communication, we employed transient EL to investigate charge carrier recombination in multilayer OLEDs. We used dye-doped CBP to work as the emissive layer. By keeping the backbone the same and changing the side groups, we were able to quantify the effect of the side groups on charge carrier recombination, and hence the device performance. The recombination coefficient (γ) of charge carriers are obtained from the decay part of transient EL through elaborate design of device structure. Our results are in good agreement with the predictions of the Langevin model of charge carrier recombination assuming the process controlled by charge carrier diffusion.²⁷ The analysis of charge carrier recombination kinetics clearly demonstrates that the donor groups and π -conjugated structure of the molecule assure high EL efficiency with the same EL spectra. Based on the results of device performance and transient EL, we discuss the relationship between γ and molecular structure, which may guide the molecule design by modification of side groups to realize highly efficient OLEDs.

The device had a molecule-doped multilayer structure with pre-cleaned indium-tin-oxide (ITO) as the anode and aluminium (Al) as the cathode. N,N'-Bis(naphthalen-1-yl)-N,N'-bis(phenyl)benzidine (NPB) and tris(8-hydroxyquinoline) aluminium (Alq₃) were used as hole and electron transport layer, respectively. 4,4'-Bis(N-carbazolyl)-1,1'-biphenyl (CBP) was employed as the host, and Bathocuproine (BCP) worked as the hole blocking layer. LiF was

deposited as the buffer layer. Dye molecules with different side groups were used as dopants (Figure 1).

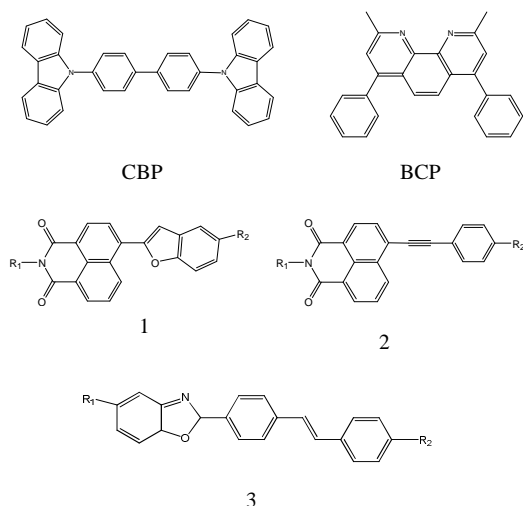


Figure 1. Chemical structures of CBP, BCP, **molecule 1:** N-alkyl-4-benzofuran-1,8-naphthalimides, **molecule 2:** N-alkyl-4-arylacetylene-1,8-naphthalimides and **molecule 3:** 2-(E)-stilbene benzoxazole. (R1 and R2 indicate side groups in the molecules).

The devices were fabricated with the structure: ITO/NPB (40 nm)/CBP:X (1 %)(20 nm)/BCP (20 nm)/Alq₃ (40 nm)/LiF (1 nm)/Al (200 nm), in which X indicated the dye molecules used in the experiments (Figure 2). All layers were prepared in a high-vacuum chamber with the pressure less than 5×10^{-4} Pa by thermal evaporation without breaking the vacuum. All organic films except dye molecules were deposited at the rate of 0.1–0.3 nm/s, and the doping (1%) was realized by controlling the rate ratio between the host and dye molecules. LiF and Al were deposited at a rate of 0.01 nm/s and 0.8–1.0 nm/s, respectively. The rate is determined by a calibrated quartz microbalance, and the active area is $3 \times 3 \text{ nm}^2$.

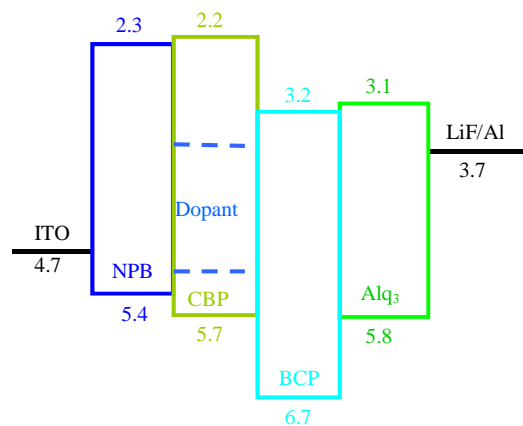


Figure 2. Device structure and energy levels for dye molecule doped multilayer OLEDs.

Current density-Luminance-Voltage (J-L-V) characteristics were measured using a Keithley sourcemeter unit (Keithley 2400 and Keithley 2000) with a calibrated silicon photodiode. The EL spectra were measured by a JY SPEX CCD3000 spectrometer. The UV-vis and PL spectra were measured using a Perkin-Elmer Lambda 35 UV-vis spectrophotometer and a Perkin-Elmer LS 50B spectrofluorometer, respectively. For the transient EL, an Agilent 8114A 100 V/2A programmable pulse generator was used to apply rectangular voltage pulse to the devices. The repetition rate of the

pulse was 1 kHz, and the pulse length was 20 μs . The time-dependent EL signals were detected by the 50 Ω input resistance of a digital oscilloscope (Agilent Model 54825A, 500 MHz/2 Gs/s) together with a photomultiplier (time resolution ≈ 0.65 ns) located directly on top of the emitting devices. All measurements were carried out at room temperature under ambient conditions.

Table 1. List of Molecule 1 with different side groups

Sample	R ₁	R ₂	$\lambda_{\text{UV, max}}$ (nm)	$\lambda_{\text{EL, max}}$ (nm)	Melt point (°C)
1a	n-Bu	t-Bu	397.0	508.5	170.0-171.5
1b	n-Bu	CH ₃	398.5	508.0	140.0-141.0
1c	n-Bu	Cl	386.5	493.0	174.5-176.0
1d	n-Hexyl	CN	378.5	470.0	213.0-214.0

The dye molecule dopants used in this experiment are derivatives of naphthalimide and stilbene, which have been reported to be very promising molecules in OLEDs. They have very good photochemical and thermal stability, and their molecule structures can be easily modified to obtain colour adjustable emission.²⁸⁻³³ We use three different dye molecules (Figure 1) in the experiments. Considering that consistent results can be drawn from these three different molecules, we focus on the discussions on Molecule 1 in the main text and leave Molecules 2 and 3 in the Supplementary Information. Table 1 summarises the physical properties of Molecule 1 with different side groups.

The device structure is shown in Figure 2 and the related energy levels are collected from the references.³⁴⁻³⁶ As shown in Figure 3a, four devices have almost the same EL spectra peaked at around 500 nm. This peak is significantly different from the peak at ~ 550 nm from pure Alq₃,³⁷ meaning that the carrier recombination is mainly confined in the molecule doping layer. At the same time, we notice that the four molecules with different side groups give very different device performance (Figure 3b). Table 2 lists the performance for all four devices. Device 1a has the highest current efficiency of 3.7 cd/A with luminance of 3640 cd/m², while Device 1d gives the lowest efficiency (less than 1 cd/A) with luminance about 760 cd/m². The performance of Devices 1b and 1c lies between that of 1a and 1d.

Table 2. List of device performance and related parameters for Molecule 1

	Slope (S)	Intercept (A)	γ ($10^{-12} \text{ cm}^3/\text{s}$)	Efficiency (cd/A)	Luminance (cd/m ²)
1a	2.25	2.22	5.80 ± 0.05	3.7	3640
1b	2.03	2.11	5.22 ± 0.05	3.0	2550
1c	3.32	4.09	3.72 ± 0.05	2.5	1040
1d	1.28	2.48	1.50 ± 0.05	0.8	760

* The unit is $10^6 (\text{cm}^3/\text{s})^{1/2}$ for S, and $(\text{cm}^3)^{1/2}$ for A.

In order to understand the operation mechanisms of the devices as well as the physics behind the significant difference between these four devices, we examined their J-V curves. As shown in Figure 4a, all the J-V characteristics follow power-law dependence, which has been proposed to be charge-trap limited transport.^{38,39} Assuming an exponential trap energy distribution, the J-V relationship can be described by $J \sim V^{m+1}$, where $m = T_t/T$ with T being the absolute temperature and T_t being the characteristic temperature of the trap distribution. The value of the exponent m is related with trap concentrations and mobility, and higher value of m means deeper traps in the devices. For all the four devices, they share an exponent value of around 9, indicating that there are similar trap distributions in the four devices. Considering the dye dopants have similar molecular structures, it is reasonable that the four devices have similar trap distributions. The fact that the current is dominated by traps also indicates that J-V curves are determined by the bulk properties rather than by contact effects.¹⁹

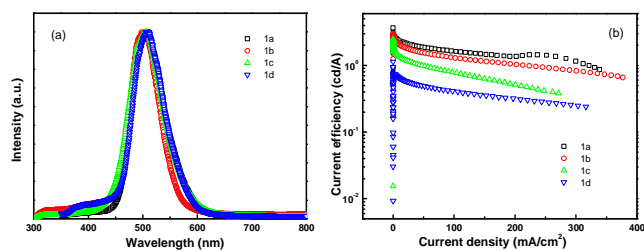


Figure 3. Device performance for dye molecule-doped multilayer OLEDs with Molecule 1 doping. (a) EL spectra and (b) Current efficiency-current density.

Further information regarding the device operation is revealed from the luminance-current density (L-J) curves. As shown in Figure 4b, all the L-J curves have a linear relationship in log-log plot with a slope of 1 at high electric fields, meaning that the devices work in the volume-controlled EL mode,¹⁹ consistent with our conclusion based on the J-V curves. Both the power-law dependence of J-V and the linear relation of L-J confirm the Langevin bimolecular recombination in the devices.²⁷ Holes injected from the ITO are transported through the hole transport layer NPB to the doping emission layer, and their transport to Alq₃ side is blocked by the BCP layer because of high injection barrier at CBP/BCP interface. Therefore, holes are confined in the doped emission layer and have to wait for the electrons to arrive. Electrons injected from LiF/Al cathode are transported through the electron transport layer Alq₃ and the hole blocking layer BCP. Electrons finally transport to the doped emission layer to recombine with the waiting holes, producing light emission from the dye molecule. The low mobility of NPB and Alq₃ make the effective transit time in the device very long, resulting in high recombination probability.^{12,19} As a result, the devices operate in the volume-limited mode.

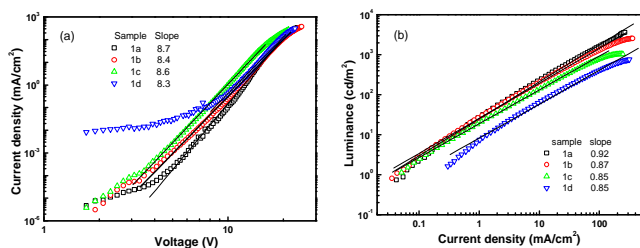


Figure 4. Steady state characterization for the devices with Molecule 1 doping. (a) Current density-voltage and (b) Luminance-current density.

For volume-limited current, with bimolecular recombination in the narrow zone of the emission layer to be the main channel for carriers decay, the free carrier kinetics can be described by the following equations:¹⁹

$$\frac{dn_h}{dt} \cong \frac{j_h}{eL_h} - \gamma n^2 \quad (1)$$

$$\frac{dn_e}{dt} \cong \frac{j_e}{eL_e} - \gamma n^2 \quad (2)$$

Where n , j and L are the charge carrier concentration, current density and the thickness of transport layer, respectively. γ is the bimolecular recombination coefficient. The subscripts h and e represent hole and electron. Here, “electron transport” layer can be approximately considered to include Alq₃ and BCP since there is almost no barrier for electron injection at the interface; “hole transport” layer includes NPB and CBP because of small barrier for hole injection and its

higher mobility. As a result, the transport layer has the same thickness of 60 nm for electrons and holes. Because $j_h = j_e = j$, the initial concentration of charge carriers is $n_0 = (j/e\gamma L)^{1/2}$ under the steady-state conditions ($L_h = L_e = L$).

Although the hole mobility in NPB is larger than the electron mobility in Alq₃, there is a high barrier at CBP/BCP interface for hole injection into Alq₃ layer. As a result, the excess holes will accumulate in doped emission layer near CBP/BCP interface. For electrons, it is easier for them to inject through BCP to the emission layer. Therefore the light-emission is dominated by the recombination in doped layer rather than in Alq₃, as confirmed by the spectra results. In addition, because of the relatively large value of the coulombic capture radius, the recombination time is substantially shorter than the trapping time. This means that the injected electrons and holes in the recombination zone will recombine rapidly, and hence no excess charge carriers exist. Consequently, except for the accumulated holes, holes as well as electrons in the recombination zone may be considered to be free and approximately equal each other in concentration ($n_h \cong n_e = n$). The charge decay after the voltage pulse is turned off can then be simplified as

$$\frac{dn}{dt} \cong -\gamma n^2 \quad (3)$$

Thus,

$$\frac{1}{n} = \frac{1}{n_0} + \gamma t \quad (4)$$

Taking into account the EL yield,

$$\Phi_{EL} = \phi_{PL} P_s \gamma [n(t)]^2 \quad (5)$$

Where ϕ_{PL} is the fluorescent quantum efficiency, P_s is the function that a singlet rather than a triplet is generated. The EL decay can then be expressed as

$$\frac{1}{\sqrt{\Phi_{EL}(t)}} = \frac{1}{\sqrt{\phi_{PL} P_s \gamma n_0^2}} + \sqrt{\frac{\gamma}{\phi_{PL} P_s}} t \quad (6)$$

This equation clearly indicates that the reciprocal of the square root of the decay EL intensity is in linear relationship with the time scale. From the ratio of slope $S = (\gamma / \phi_{PL} P_s)^{1/2}$ to intercept

$A = (\phi_{PL} P_s \gamma n_0^2)^{-1/2}$, the electron-hole recombination coefficient then can be calculated as:

$$\gamma = \frac{(S/A)^2 eL}{j} \quad (7)$$

Equation 7 enables us to investigate the charge carrier recombination immediately after switching off the bias. Therefore, here we employed transient EL to investigate charge carrier recombination in the devices, aiming to further understand the difference between these four devices.

Figure 5a shows the relationship of transient EL intensity-time in dye molecule-doped OLEDs at the same equilibrium current of 170 mA/cm², and it shows different EL decay for devices with different doping molecules, providing useful information on charge carrier recombination in different devices. In order to quantify the charge carrier recombination, we further plot the transient EL decay $(\Phi_{EL})^{-1/2}$ versus time in Figure 5b, where the inset shows the $\Phi_{EL}(t)$ decay curves. Here $t=0$ corresponds to the voltage fall of the pulse. Perfect straight lines can be fitted to the experimental data withing experimental error range. The values of slopes (S) and intercepts (A) are obtained from the linear relationship, and then the charge carrier recombination coefficient γ can be calculated with $j=170$ mA/cm² and $L=60$ nm (refer to Equation 7). The values are

summarised in Table 2. The device with Molecule 1a doping has shown the highest γ of $(5.80 \pm 0.05) \times 10^{-12} \text{ cm}^3/\text{s}$, which is nearly four times of the lowest value of $(1.50 \pm 0.05) \times 10^{-12} \text{ cm}^3/\text{s}$ for the device with Molecule 1d doping. As well known, high γ means that highly efficient recombination of holes and electrons in the devices. Therefore the fitted γ values are consistent with the device performance, with the device with Molecule 1a showing the highest efficiency. Considering that the only difference between different molecules lies in the side groups, it is reasonable to conclude that the difference in EL efficiency may result from the side groups. As reported before, donor group (e.g. in Molecule 1a) is considered to form strong push-pull electron structure, and hence the electron can easily transfer to the aromatic ring to form expanded π -conjugated structure, enhancing fluorescence emission from the molecule backbone,^{28,29} while strong acceptor group (e.g. in Molecule 1d) will decrease the fluorescence emission as it reduces the electron density in the system. Indeed, in our experiments, donor groups assure higher EL efficiency for the molecule-doping multilayer OLEDs, and the higher γ values are consistent with the device results.

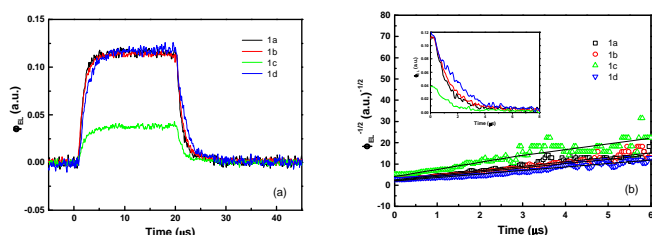


Figure 5. Transient EL characterization for the devices with Molecule 1 doping. (a) Transient EL intensity-time and (b) comparison of the transient EL decay at the same equilibrium current density of $170 \text{ mA}/\text{cm}^2$ plotted in $(\phi_{EL})^{-1/2}$ versus time scale. The $\phi_{EL}(t)$ decay curves are shown in the inserted. Here $t=0$ corresponds to the voltage fall of the pulse.

We have also extended our measurements to other molecules to generalise our observations. For Molecule 2, we obtain similar results and conclusions as Molecule 1 (see supplementary Figures s1 and s2), in which the donor groups, such as $-\text{CH}_3$, guarantee higher γ and EL efficiency, while the acceptor groups, such as $-\text{F}$ and $-\text{CF}_3$, decrease the γ and EL efficiency. Molecule 3, though a little bit complicated, also shows results consistent with Molecules 1 and 2. R_1 group shows stronger donor in 3a and 3b (t-Bu) than in 3c ($-\text{H}$). In addition, R_2 group, $-\text{COOCH}_3$ (3a) and $p\text{-C}_6\text{H}_5$ (3b) can bring bigger π -conjugated structure than 2,5- OCH_3 (3c) in the backbone. Therefore, more delocalized electrons can be excited, and then the devices with Molecules 3a and 3b show higher γ and EL efficiency compared with Molecule 3c (Figure s3 and s4).

In conclusion, multilayer OLEDs was designed and fabricated based on molecule-doping technology, in which derivatives of naphthalimide and stilbene with different side groups were used as the dopants in CBP host as the light-emission layer. All devices for each set of molecules showed almost the same EL spectra, but very different efficiency. Transient EL, by which the kinetics of the charge carrier recombination was investigated, was used to understand the physics behind the different EL efficiency. The coefficient (γ) of electron-hole recombination was determined from the long-time component of the temporal decay of the EL intensity after a rectangular voltage pulse was turned off. It was found that γ and EL efficiency were both strongly dependent on the side groups of the dopants. Donor structures in the side groups guarantee much higher γ and EL efficiency than the acceptor ones. Our results provide a promising guide for the structure design for molecular materials in highly efficient OLEDs. Chemists can slightly change the side groups to maintain the desired emission spectra while

significantly enhance the device efficiency. In addition, this report may provide useful hints on how to design molecule structure to reduce charge carrier recombination, which is considered to be the main cause of efficiency loss in organic solar cells.⁴⁰⁻⁴²

Acknowledgements

We thank Prof. Longhe Xu from Dalian University of Technology to provide the molecules. Dr. Ma thanks the financial support of Hundreds Talents Program, Chinese Academy of Sciences and the National Science Fund for Distinguished Young Scholars of China (50325312). F.G. acknowledges the financial support of the European Commission under a Marie Curie Intra-European Fellowship for Career Development.

Notes and references

^a State Key Laboratory of Polymer Chemistry and Physics, Changchun Institute of Applied Chemistry, Chinese Academy of Sciences, 130022, Changchun, China.

^b Department of Physics, Chemistry and Biology, Linköping University, SE-58183 Linköping, Sweden

^c State Key Laboratory of ASIC and System, Department of Microelectronics, SIST, Fudan University, 200433, Shanghai, China

* shesh@ifm.liu.se

† Electronic Supplementary Information (ESI) available: Experimental results for dye molecule-doped multilayer OLEDs with other molecular systems (2 and 3) are provided as well by use of steady state and transient EL characterization to support the conclusion and discussion in the main text. See DOI: 10.1039/c000000x/

- G. Gustafsson, Y. Cao, G.M. Treacy, F. Klavetter, N. Colaneri and A. J. Heeger, *Nature* 1992, **357**, 477-479.
- B. W. D'Andrade and S. R. Forrest, *Adv. Mater.* 2004, **16**, 1585-1595.
- S. Reineke, F. Lindner, G. Schwartz, N. Seidler, K. Walzer, B. Lussem and K. Leo, *Nature* 2009, **459**, 234-238.
- L. Xiao, Z. Chen, B. Qu, J. Luo, S. Kong, Q. Gong and J. Kido, *Adv. Mater.* 2011, **23**, 926-952.
- M. C. Gather, A. Köhnen and K. Meerholz, *Adv. Mater.* 2011, **23**, 233-248.
- G. Schwartz, S. Reineke, T.C. Rosenow, K. Walzer and K. Leo, *Adv. Funct. Mater.* 2009, **19**, 1319-1333.
- W. Brütting, S. Berleb and A. G. Muckl, *Org. Electron.* 2001, **2**, 1-36.
- M. A. Baldo and S. R. Forrest, *Phys. Rev. B* 2001, **64**, 085201.
- J. C. Scott, *J. Vac. Sci. Technol. A* 2003, **21**, 521-531.
- G. G. Malliaras and J. C. Scott, *J. Appl. Phys.* 1998, **83**, 5399-5403.
- Y. Shirota and H. Kageyama, *Chem. Rev.* 2007, **107**, 953-1010.
- T. C. Wong, J. Kovac, C. S. Lee, L. S. Hung and S. T. Lee, *Chem. Phys. Lett.* 2001, **334**, 61-64.
- S. Barth, P. Müller, H. Reil, P. F. Seidler, W. Rieß, H. Vestweber and H. Bassler, *J. Appl. Phys.* 2001, **89**, 3711-3719.
- H. Chayet, R. Pogreb and D. Davidov, *Phys. Rev. B* 1997, **56**, R12702.
- P. W. M. Blom and M. C. J. M. Vissenberg, *Phys. Rev. Lett.* 1998, **80**, 3819-3822.

- 16 D. J. Pinner, R. H. Friend and N. Tessler, *J. Appl. Phys.* 1999, **86**, 5116-5130.
- 17 Y. H. Tak, J. Pommerehne, H. Vestweber, R. Sander, H. Bassler and H. H. Horhold, *Appl. Phys. Lett.* 1996, **69**, 1291-1293.
- 18 J. Chen and D. Ma, *J. Appl. Phys.* 2004, **95**, 5778-5781.
- 19 J. Kalinowski, N. Camaioni, P. Di Marco, V. Tattori and A. Martelli, *Appl. Phys. Lett.* 1998, **72**, 513-515.
- 20 J. Chen and D. Ma, *J. Phys. D: Appl. Phys.* 2006, **39**, 2044-2047.
- 21 J. Chen, D. Ma, Y. Liu and Y. Wang, *J. Phys. D: Appl. Phys.* 2005, **38**, 3366-3370.
- 22 M. A. Baldo and S. R. Forrest, *Phys. Rev. B* 2000, **62**, 10958-10966.
- 23 J. H. Park, C. Yun, M. H. Park, Y. Do, S. Yoo and M. H. Lee, *Macromolecules* 2009, **42**, 6840-6843.
- 24 S. E. Shaheen, G. E. Jabbour, B. Kippelen, N. Peyghambarian, J. D. Anderson, S. R. Marder, N. R. Armstrong, E. Bellmann and R. H. Grubbs, *Appl. Phys. Lett.* 1999, **74**, 3212-3214.
- 25 C. Rothe, C. J. Chiang, V. Jankus, K. Abdullah, X. Zeng, R. Jitchati, A. S. Batsanov, M. R. Bryce and A. P. Monkman, *Adv. Funct. Mater.* 2009, **19**, 2038-2044.
- 26 S. Setayesh, A. C. Grimsdale, T. Weil, V. Enkelmann, K. Mullen, F. Meghdadi, E. J. W. List and G. Leising, *J. Am. Chem. Soc.* 2001, **123**, 946-953.
- 27 M. Pope and C. E. Swenberg, *Electronic Processes in Organic Crystals*, Oxford University Press, Oxford 1982.
- 28 J. X. Yang, X. L. Wang, X. M. Wang and L. H. Xu, *Dyes Pigm.* 2005, **66**, 83-87.
- 29 J. X. Yang, X. L. Wang, S. Tong and L. H. Xu, *Dyes Pigm.* 2005, **67**, 27-33.
- 30 P. Wang, Z. Xie, S. Tong, O. Wong, C.S. Lee, N. Wong, L. Hung and S. T. Lee, *Chem. Mater.* 2003, **15**, 1913-1917.
- 31 W. Zhu, L. Fan, R. Yao, F. Wu and H. Tian, *Synt. Met.* 2003, **137**, 1129-1130.
- 32 A. Kukhta, E. Kolesnik, M. Taoubi, D. Drozdova and N. Prokopchuk, *Synt. Met.* 2001, **119**, 129-130.
- 33 I. Fuks-Janczarek, I. V. Kityk, R. Miedzinski, E. Gondek, J. Ebothe, L. Nzoghe-Mendome and A. Danel, *J. Mater. Sci. Mater. Electron.* 2007, **18**, 519-526.
- 34 S. Shi and D. Ma, *Semicond. Sci. Technol.* 2005, **20**, 1213-1216.
- 35 M. A. Baldo, S. Lamansky, P. E. Burrows, M. E. Thompson and S. R. Forrest, *Appl. Phys. Lett.* 1999, **75**, 4-6.
- 36 T. Zhang, Y. Liang, J. Cheng and J. Li, *J. Mater. Chem. C* 2013, **1**, 757-764.
- 37 C. W. Tang and S. A. VanSlyke, *Appl. Phys. Lett.* 1988, **51**, 913-915.
- 38 P. E. Burrows, Z. Shen, V. Bulovic, D. M. McCarty, S. R. Forrest, J. A. Cronin and M. E. Thompson, *J. Appl. Phys.* 1996, **79**, 7991-8006.
- 39 L. S. Hung, C. W. Tang and M. G. Mason, *Appl. Phys. Lett.* 1997, **70**, 152-154.
- 40 S. R. Cowan, N. Banerji, W. L. Leong and A. J. Heeger, *Adv. Funct. Mater.* 2012, **22**, 1116-1128.
- 41 C. M. Proctora, M. Kuika and T. Q. Nguyen, *Prog. Polym. Sci.* 2013, **38**, 1941-1960.
- 42 F. Gao and O. Inganäs, *Phys. Chem. Chem. Phys.* 2014, **16**, 20291-20304.

The table of contents entry: Effects of side groups on kinetics of charge carrier recombination are investigated in dye molecule-doped multilayer organic light-emitting diodes by transient electroluminescence.

ToC figure

